Multi-rate Nonlinear Control for Enhancing the Servo Performance of HDD Systems

Minghui Zheng

Xu Chen

Masayoshi Tomizuka

CML Sponsors' Meeting 2013

University of California, Berkeley

Contents

1. Introduction

In hard disk drives (HDDs), vibrations caused by abrupt control input variations and other external disturbances would affect the servo performance seriously and limit the application of HDDs in modern multimedia devices. Nonlinear control techniques can be potentially applied to enhance servo performance of HDDs.

One promising algorithm is to combine sliding mode controller and nonlinear PID controller to enhance the transient performance. When the tracking error is large, sliding mode control and nonlinear PID control work together to rapidly reduce the error; when the error is small, sliding mode control is turned off to ensure good steady state performance. As to the nonlinear PID, the tracking error signal will be utilized to tune the nonlinear integral gain and nonlinear derivative gain, aiming to (1) shorten the settling time, (2) reduce the peak error, and (3) keep the good steady state performance.

Another promising algorithm is the pure discrete-time sliding mode control. Sliding mode control has strong robustness to large disturbance and model uncertainty. By unifying tasks such as track-seeking and track-following into one control scheme, sliding mode control would perhaps reduce possible vibrations caused by the switching between different control schemes. Furthermore, considering its high frequency property, sliding mode control can be a promising method to inhibit vibrations, if necessary computations, for example control law and state estimation, can be handled efficiently in HDDs.

In most HDDs, the Position Error Signal (PES) sampling rate is highly restricted by the number of servo wedges/sectors, but the control signal can be updated at a faster rate. One potential approach would be to use multi-rate control techniques to increase the sampling rate of other aspects of the system, such as the control signal. Such a multi-rate approach can help mitigate vibrations and enhance the servo performance by reducing the change of control input at each sampling instance. Combining the aforementioned ideas together, multi-rate nonlinear control can be utilized for enhanced vibration rejection especially in the steady-state performances of HDDs.

This project aims at developing control schemes that can break current performance limitations during both track-seeking and track-following processes in HDDs. More specifically, by unifying different tasks into one control scheme, we aim to reduce the vibrations caused by abrupt control updates; by increasing the sampling rate of control signals, we seek to develop algorithms to break the bandwidth limitation so as to enhance the resistance to shocks, external vibrations, etc.,. Limited results on multi-rate nonlinear control exist in current research literatures. We plan to further develop the multi-rate nonlinear control technology and extend its application from single-stage to dual-stage HDD products, where the micro actuator has promising structural superiorities for control engineering.

2. Benchmark Model

The control algorithm studied in this project is based on the Benchmark Model [1]. The frequency response of the nominal model and the full-order model are illustrated as follows.

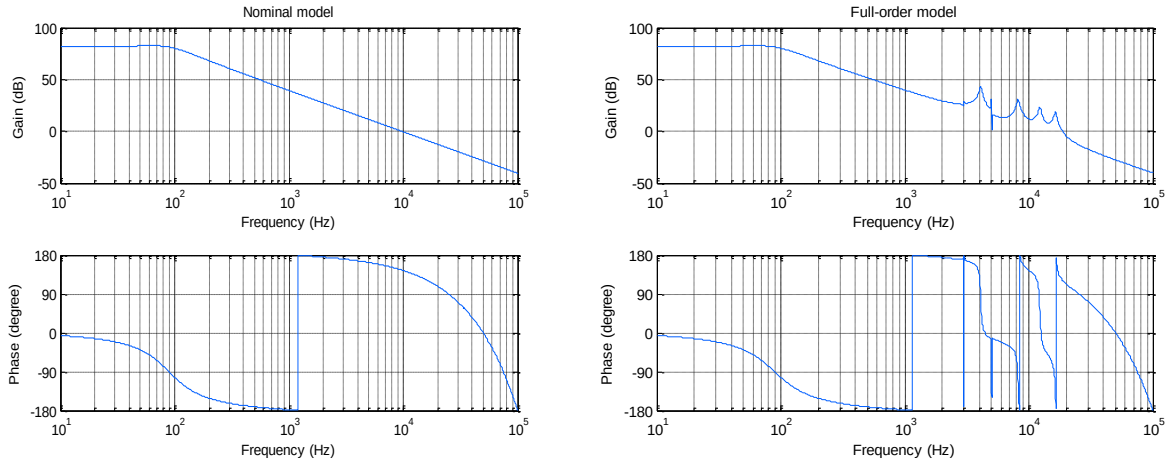

a. Nominal Model b. Full-order Model

Figure 2.1 Bode Diagram of HDD Model from Benchmark

The Benchmark Model also includes a disturbance profile, including the force disturbance, flutter disturbance, sensor noise and repeatable run-out (RRO) disturbance. The disturbances in both the frequency domain and the time domain are illustrated as follows.

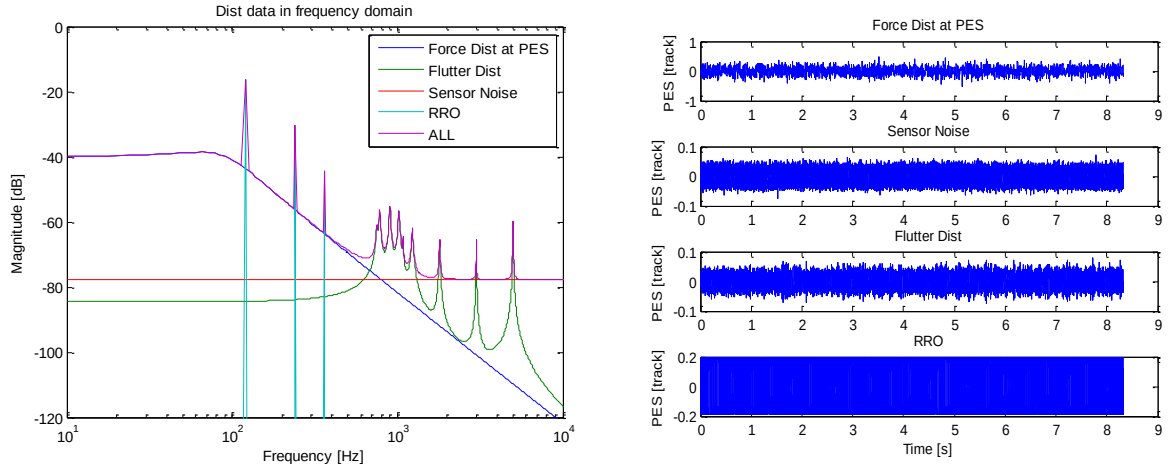

a. Frequency Domain b. Time Domain

Figure 2.2 Disturbance Data from Benchmark

The whole control system is shown as follow, which includes the plant, the controller and the state observer.

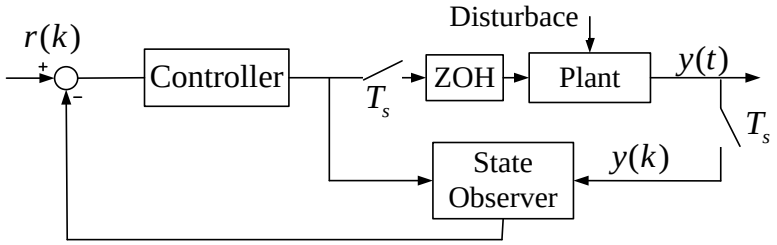

Figure 2.3 Control System

Some physical parameters in the Benchmark model are listed as in Table 2.1.

Table 2.1 Parameters of the Benchmark Model	
PES sampling rate	$T_s = 3.7879 \times 10^{-5}$ s
Position measurement gain	$k_y = 3.937 \times 10^{6}$ track $\cdot$ m^{-1}
Acceleration constant	$k_v = 951.2$ ms^{-2}A^{-1}
Rotational speed	$r = 7200$
Number of servo sectors per track	$n = 220$
Width of track	$T_p = 2.54e-7$ m

References

[1] http://mizugaki.iis.u-tokyo.ac.jp/nss/

3. Introduction to Sliding Mode Control (SMC)

Sliding mode control is a central approach used in this project. This section provides a brief overview of the theoretical backgrounds.

Consider the system

$$\dot{e} = f(e) + b(e)u \tag{3.1}$$

where $e = [e_1 \; e_1^{(1)} \ldots e_1^{(n-1)}]^T = [e_1 \; \frac{de_1}{dt} \ldots \frac{d^{(n-1)}e_1}{dt^{(n-1)}}]^T$, e_1 is PES, $f(e)$ and $b(e)$ are nonlinear or linear functions, and u is the control signal.

Define

$$s(e;t) = (\frac{d}{dt} + \lambda)^{n-1} e_1 \tag{3.2}$$

where λ is a strictly positive constant. Specially, for $n = 2$,

$$s(e;t) = \dot{e}_1 + \lambda e_1 \tag{3.3}$$

Noting that $s(e;t) \equiv 0$ represents a linear differential equation whose unique solution is $e_1 \equiv 0$. Denote the set as $S \triangleq \{e \mid s(e;t) \equiv 0\}$. One of the advantages of sliding mode control is to transform an nth-order tracking problem over e into a 1st-order stabilization problem over s.

The control signal u can be designed to realize that, when s is outside of S,

$$\frac{1}{2}\frac{d}{dt}s^2 \le -\eta |s| \tag{3.4}$$

where $\eta > 0$. Equation (3.4) is known as the sliding condition. This implies the sliding surface $s = 0$ will be reached in a finite time shorter than $|s(0)|/\eta$. That is, $t_{phaseI} \le |s(0)|/\eta$. After hitting the sliding surface, the tracking error converges exponentially to zero, with a time constant $(n-1)/\lambda$.

A boundary layer, defined by $\{s : |s| = \phi\}$ with thickness ϕ, is usually introduced to inhibit the chatter caused by the sliding mode control. The relationship between the thickness of the layer and the magnitude bound of the actual errors can be obtained as follow:

$$\forall t \ge t_0, |s(t)| \le \phi \Rightarrow \forall t \ge t_0, |e^{(i)}(t)| \le (2\lambda)^i \varepsilon, i = 0,1,2,\ldots,n \tag{3.5}$$

where $\varepsilon = \phi / \lambda^{n-1}$. Detailed derivations are provided in Reference [1].

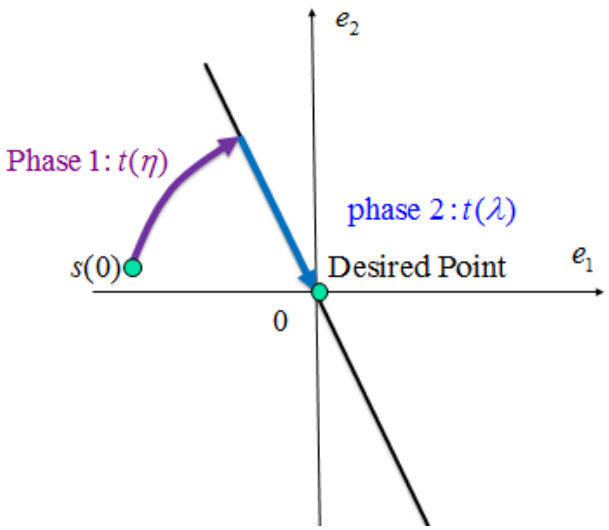

Figure 3.1 Approaching phases (Phase 1) and Sliding phase (Phase 2)

Reference

[1] Jean-Jacques E. Slotine, Werping Li, Applied nonlinear control, Prentice Hall, 1991

4. Nonlinear PID Combined with Sliding Mode Control

4.1 Basic Idea

Sliding Mode Control is well-known for its high-gain control nature and good robustness, but it has several disadvantages such as chatter and less direct control over steady-state performance. Therefore, in this section, the following combination of the SMC and the nonlinear PID control is proposed: when PES is large, the sliding mode control and the nonlinear PID control work together to rapidly reduce the error; when PES is small, the sliding mode control is turned off to ensure good steady state performance. As the PES becomes smaller, the nonlinear PID is reduced to a linear PID to keep the good steady state performance of a baseline PID control. The basic idea can be illustrated in Figure 4.1.

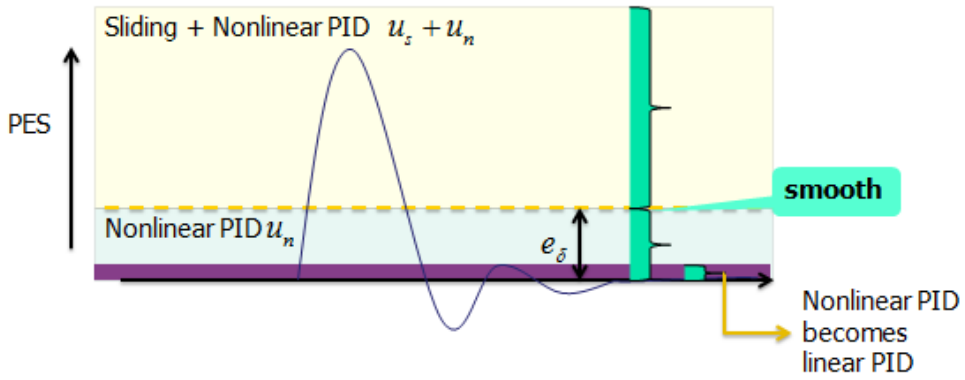

Figure 4.1 Basic Idea of Nonlinear PID and Sliding Mode Control

The whole controller structure can be expressed as

$$u = u_n(e_1) + \rho(e_1)u_s(e_1) \tag{4.1}$$

where e_1 is PES, $u_n(e_1)$ is the nonlinear PID controller, $u_s(e_1)$ is the sliding mode controller, $\rho(e_1)$ is a scaling coefficient to control the contribution of SMC, respectively. Based on the idea in the previous paragraph, we design $\rho(e_1)$ as follow

$$\rho(e_1)=\begin{cases} 0 & |e_1(k)|\le e_\delta \\ \big|\,|e_1(k)|-e_\delta\big| & |e_1(k)|> e_\delta \end{cases} \tag{4.2}$$

and we design $u_n(k)$ and $u_s(k)$ as follows

$$u_n(k)=K_p e_1(k)+K_i(e_1(k))e_i(k)+K_d(e_1(k))e_d(k) \tag{4.3}$$

$$u_s(k)=K_s sat(s(k)/\phi) \tag{4.4}$$

where $s(k)=c(e_1(k))e_1(k)+e_d(k)$; $e_d(k)=(e_1(k)-e_1(k-1))/T_s$ is the derivative of $e_1(k)$; and $e_i(k)=T_s\sum_{j=0}^{k}e_1(j)$ is the integration of $e_1(k)$.

Remarks:

1. $\rho(e_1)=0$ when $|e_1(k)|=e_\delta$, and $u_s(e_1)$ is turned off when $|e_1(k)|\le e_\delta$. This can realize the smooth turn-off of the sliding mode control.

2. The $sign(s(k))$ has been replaced by the $sat(s(k)/\phi)$ to inhibit chatter.

3. $K_i(e_1(k))$ and $K_d(e_1(k))$ are selected to be error based functions to obtain small overshoots and fast transient.

4.2 Remarks on Parameter Tuning

In this section, three parameters $K_i(e_1(k))$, $K_d(e_1(k))$, and $c(e_1(k))$ are analyzed.

First, consider the design of $K_i(e_1(k))$ to yield small overshoot, fast transient, and good steady-state performance. Several literature results [1-2] have suggested the following design concept: when the tracking error is small, $K_i(e_1(k))$ is preferred to be large; when error is large, $K_i(e_1(k))$ can be small. Therefore we choose

$$K_i(e_1(k)) = K_{i0}(1-\alpha_i \sec h(\beta_i / e_1(k)^2) \tag{4.5}$$

Denote $g_i(e_1(k)) = 1-\alpha_i \sec h(\beta_i / e_1(k)^2)$. After K_{i0} design, we would like to tune K_i slightly through $g_i(e_1(k))$. The relationship between $g_i(e_1(k))$ and $e_1(k)$ has been illustrated in Figure 4.2. When $e_1(k)$ is small, $g_i(e_1(k))$ is 1 and the nonlinear $K_i(e_1(k))$ reduced to a constant K_{i0}.

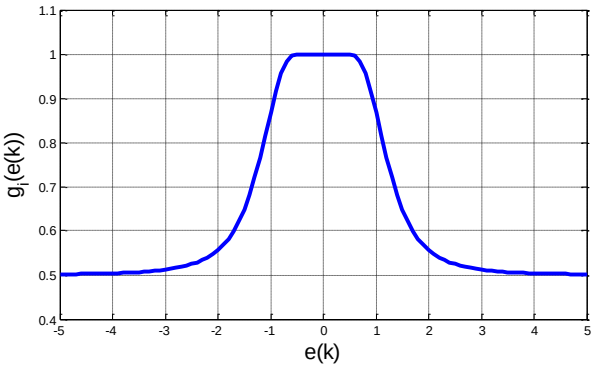

Figure 4.2 $g_i(e_1(k))$ and $e_1(k)$

As to the design of $K_d(e_1(k))$ to reduce the response time, $K_d(e_1(k))$ is preferred to be large when error is large and increasing; $K_d(e_1(k))$ is preferred to be small when error is large and decreasing. Such a tuning rule is illustrated in Figure 4.3. Based on this idea, $K_d(e_1(k))$ is designed as [1]:

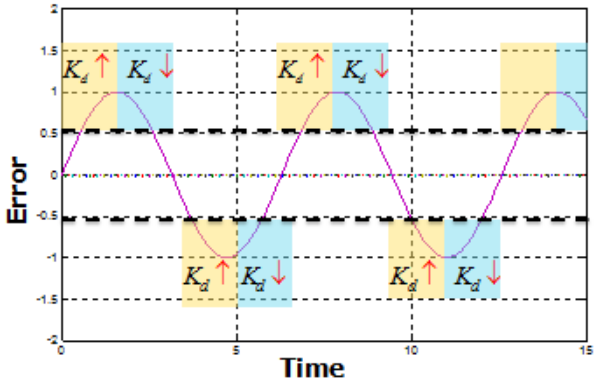

Figure 4.3 $K_d(e_1(k))$

$$K_d(e_1(k)) = \begin{cases} K_{d0}\left(1+\alpha_d \sec h(\beta_d / e_1(k)^2)\right) & if\ e_1(k)e_d(k) > 0 \\ K_{d0}\left(1-\alpha_d \sec h(\beta_d / e_1(k)^2)\right) & if\ e_1(k)e_d(k) < 0 \end{cases} \tag{4.6}$$

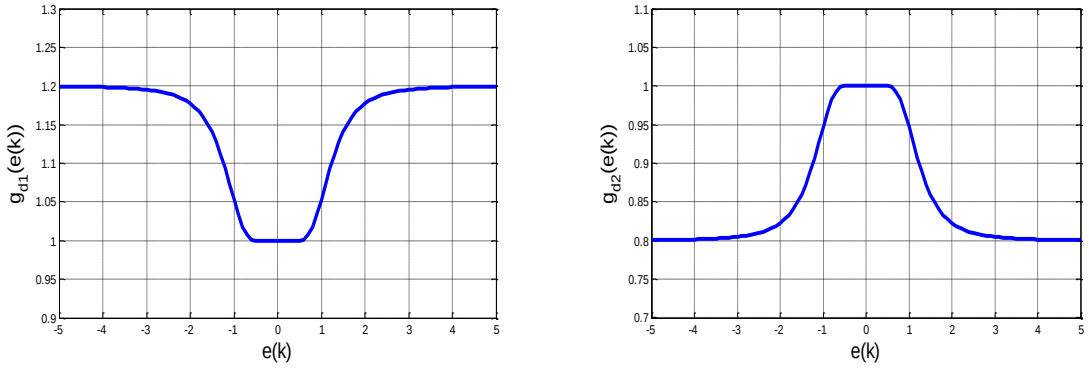

Figure 4.4 $g_{d1,2}$ *and* $e_1(k)$

Denote $g_{d1} = 1+\alpha_d \sec h(\beta_d / e_1(k)^2)$ and $g_{d2} = 1-\alpha_d \sec h(\beta_d / e_1(k)^2)$, as shown in Figure 4.4.

When $e_1(k)$ is small, we can see that $g_{d1,2}(e_1(k))$ reduce to 1 and $K_d(e_1(k))$ becomes a constant K_{d0}.

Additionally, $c(k)$ is designed as a error-based function,

$$c(e_1(k)) = \begin{cases} k_m u_{\max} / |e_1(k)| & if\ |e_1(k)| > c_\delta \\ k_m u_{\max} / c_\delta & otherwise \end{cases} \tag{4.7}$$

where k_m, $u_{\max}$, and c_δ are design parameters.

To summarize, the whole controller can be expressed by the following equations:

$$u = u_n(e_1) + \rho(e_1)u_s(e_1)$$

where

$$\rho(e_1) = \begin{cases} 0 & |e_1(k)| \le e_\delta \\ \left| |e_1(k)| - e_\delta \right| & |e_1(k)| > e_\delta \end{cases}$$

$$u_n(k) = K_p e_1(k) + K_i(e_1(k))e_i(k) + K_d(e_1(k))e_d(k)$$

$$u_s(k) = K_s sat(s(k)/\phi)$$

$$s(k) = c(k)e_1(k) + e_d(k)$$

$$c(e_1(k)) = \begin{cases} k_m u_{\max} / |e_1(k)| & if\ |e_1(k)| > c_\delta \\ k_m u_{\max} / c_\delta & otherwise \end{cases}$$

$$K_i(e_1(k)) = K_{i0}(1 - \alpha_i \sec h(\beta_i / e_1(k)^2)$$

$$K_d(e_1(k)) = \begin{cases} K_{d0}\left(1 + \alpha_d \sec h(\beta_d / e_1^2(k))\right)\ if\ e_1(k)e_d(k) > 0 \\ K_{d0}\left(1 - \alpha_d \sec h(\beta_d / e_1^2(k))\right)\ if\ e_1(k)e_d(k) < 0 \end{cases}$$

4.3 Simulation Results

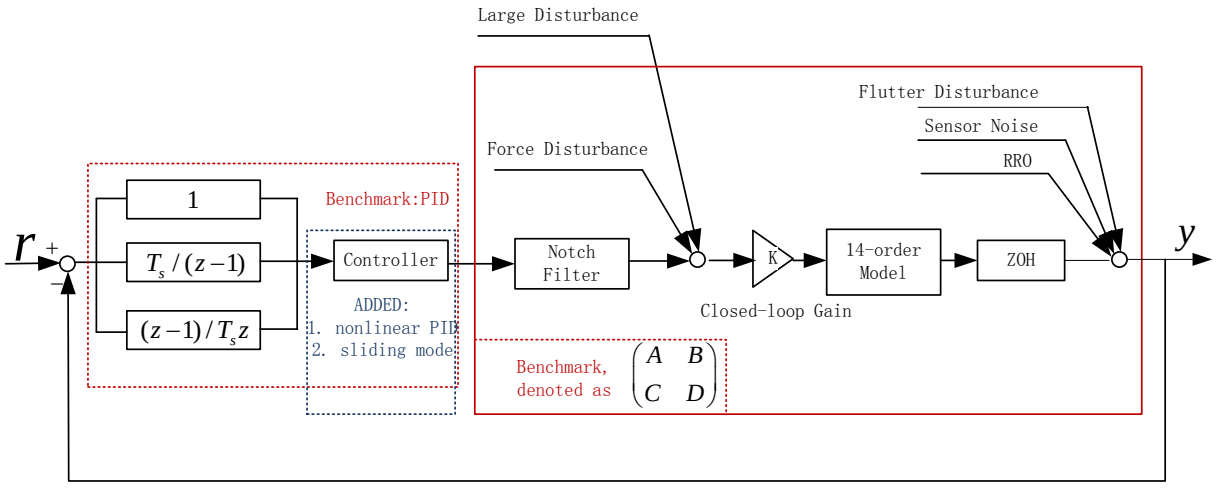

Figure 4.5 Control System

To examine the transient performance and the resistance against sudden large disturbance of the control algorithm, some simulation results are provided in this section. The whole system for simulation is shown in Figure 4.5. It includes the full-order model, the notch filters, and the disturbance profile from the

Benchmark. Additionally, large impulse input disturbance has been added to evaluate the performance. The simulation parameters are listed in Table 4.1.

Table 4.1 Simulation Parameters	
Coefficient of sliding mode control $\rho(e_1)$	$e_\delta = 0.05$
Sliding mode controller u_s	$\phi = 0.05$ $K_s = 2$
Sliding surface $s(k)$	$c_\delta = 0.2$ $u_{\max} = 0.25$ $k_m = 8$
Nonlinear PID control u_n	$K_p = 2$ $K_{i0} = 0.05; \alpha_i = 0.5; \beta_i = 2$ $K_{d0} = 70; \alpha_d = 0.2; \beta_d = 2$

For all the figures in this section, the X-axis unit is 'time / s' and the Y-axis unit is 'position / track'.

(a) Effect of $K_i(e_1(k))$

To analyze how the nonlinear $K_i(e_1(k))$ affects the performance, the simulation results for systems with nonlinear $K_i(e_1(k))$ and constant K_{i0} are compared in Figures 4.6 and 4.7. It shows that the system with nonlinear $K_i(e_1(k))$ has reduced response time in Figure 4.6; while it still keeps good steady-state performance in Figure 4.7.

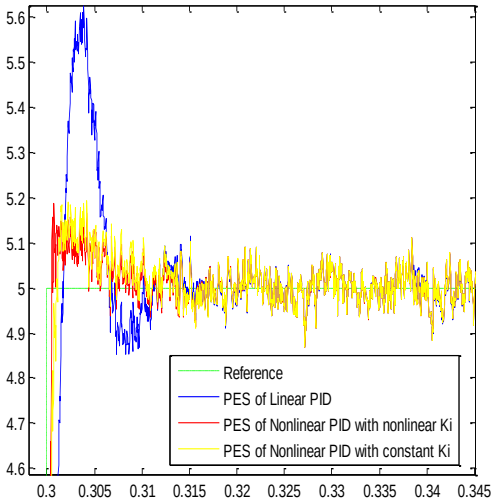

Figure 4.6 Track-Seeking with step input

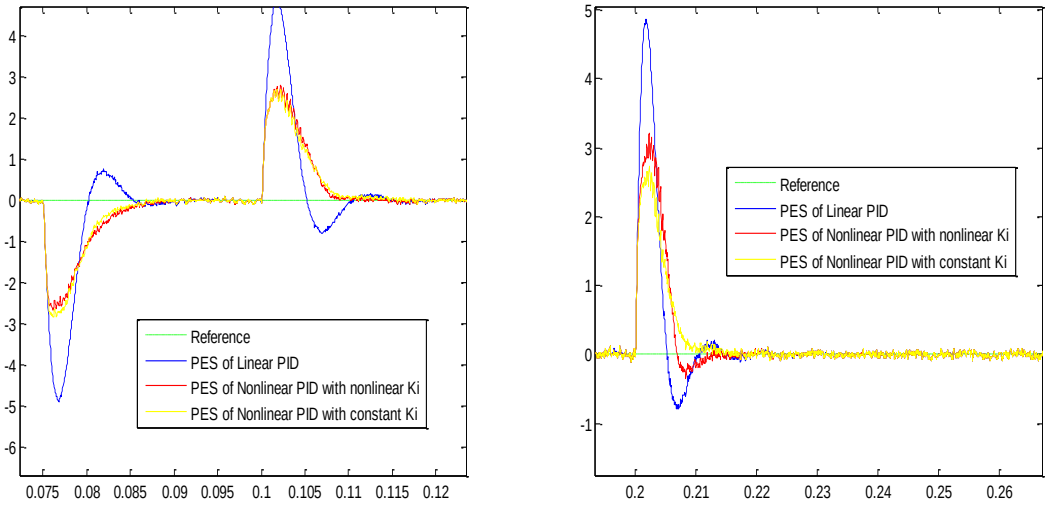

Figure 4.7 Track-following with large input disturbance

(b) Effect of $K_d(e_1(k))$

Analogous to the previous paragraph, the simulation results of the systems with the nonlinear $K_d(e_1(k))$ and a constant K_{d0} are compared in Figures 4.8 and 4.9. It is shown that the system with nonlinear

$K_d(e_1(k))$ has reduced response time and smaller overshoot in Figure 4.8, while it still keeps good steady-state performance in Figure 4.9.

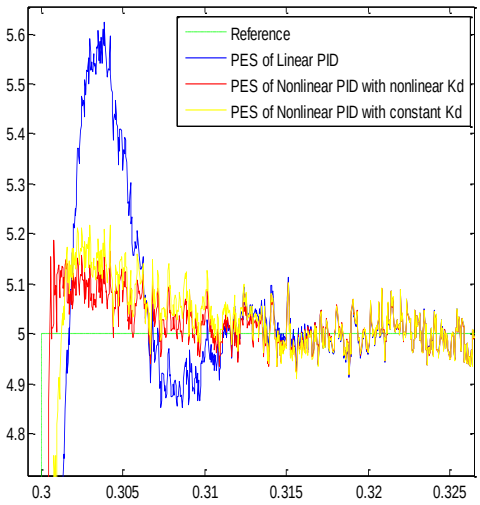

Figure 4.8 Track-Seeking with input

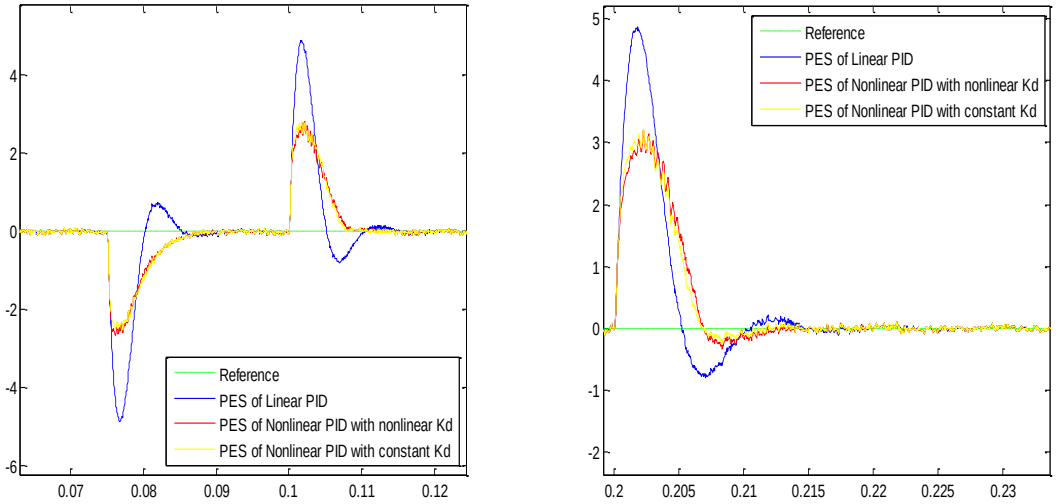

Figure 4.9 Track-following with large input disturbance

As mentioned before, the track-seeking performance can be further improved if $c(e_1(k))$ is designed properly. Simulation results among different controllers are compared in Figures 10 and 11: linear PID, nonlinear PID plus SMC with time-varying sliding surface, nonlinear PID plus SMC with time-invariant

sliding surface, linear PID plus SMC with time-varying sliding surface, and linear PID plus SMC with time-invariant sliding surface. The simulation results indicate that the nonlinear PID plus SMC with time-varying sliding surface performs best in the track-seeking process, and keeps good robustness in the track-following process.

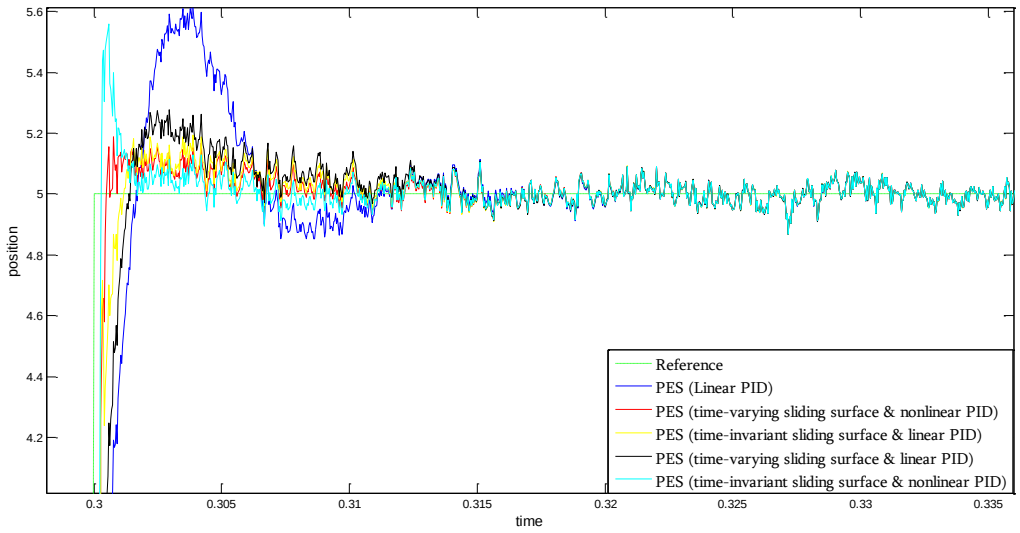

Figure 4.10 Track-Seeking Performance with Large Disturbance

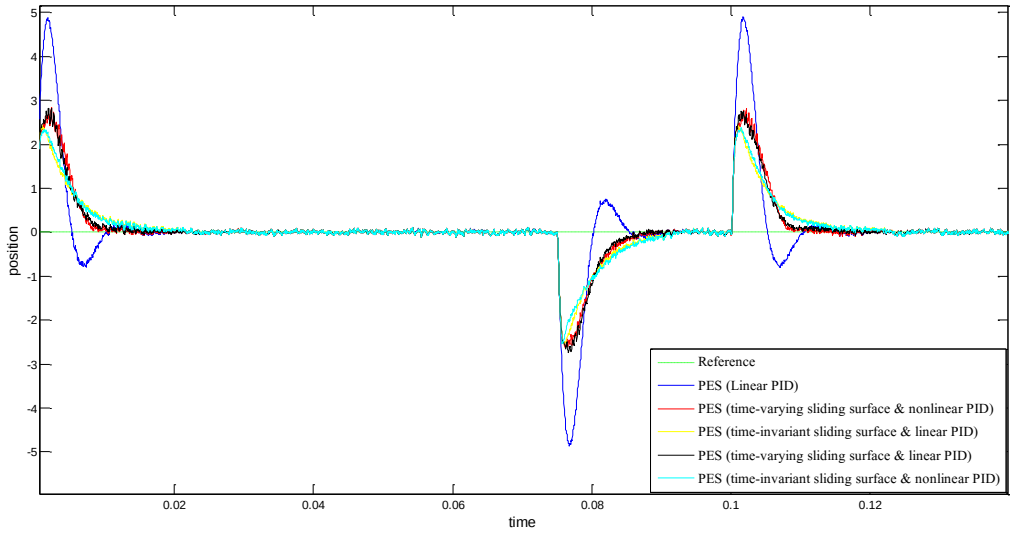

Figure 4.11 Track-Following Performance with Large Disturbance

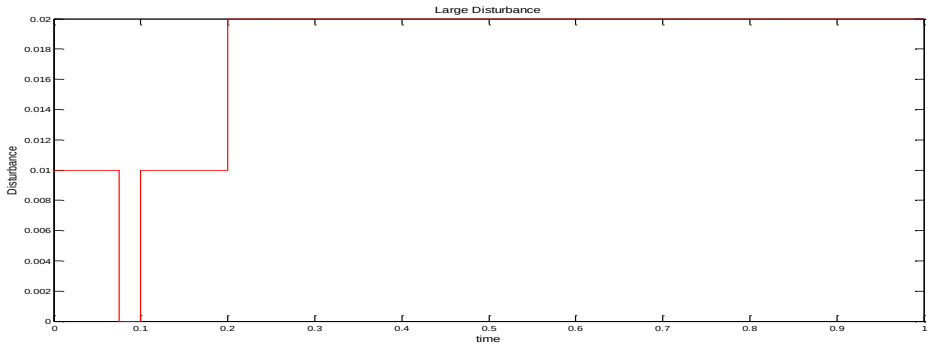

(a) Large Input Disturbance

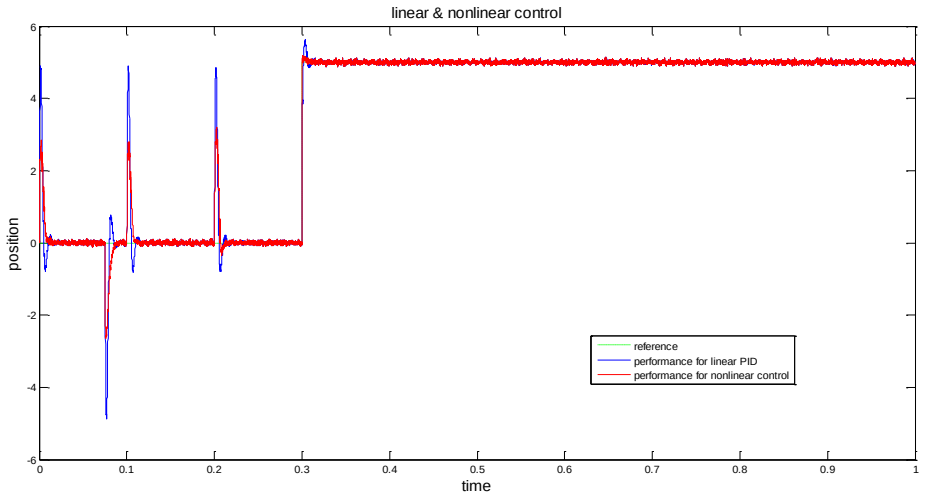

(b) Position Signal (from 0s to 1s)

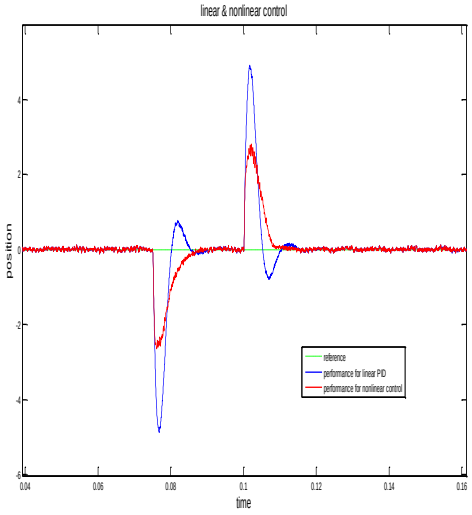

(c) Position Signal (from 0.04s to 0.16s)

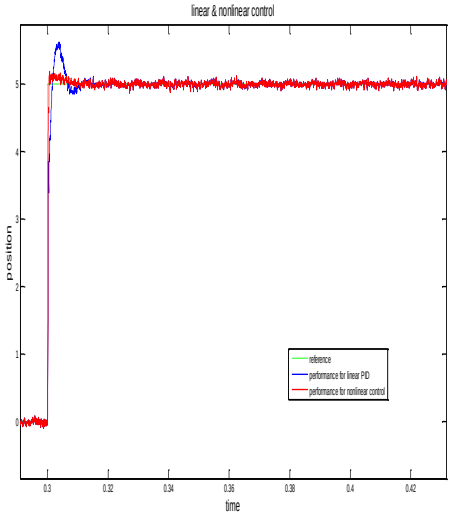

(d) Position Signal (from 0.29s to 0.43s)

Figure 4.12 Nonlinear PID combined with Sliding Mode Control

In Figure 12, the overall tack-following and track-seeking performances have been compared between the PID controller and the nonlinear controller described in Equation (4.1).

Some remarks are obtained from the simulation.

1. Compared with the original PID controller, the nonlinear controller has stronger resistance to sudden disturbances. Furthermore, it can obtain smaller overshoot and faster response during the track-seeking process.

2. The parameters in K_i and K_d should be tuned very carefully. If not, either the performance or the control signal may become worse.

3. The stability proof is difficulty due to the nonlinearity of the controller.

References

[1] Basel M. Isayed and Muhammad A. Hawwa, "A Nonlinear PID Control Scheme for Hard Disk Drive Servo systems", 2007 Mediterranean Conference on Control and Automation, July, 2007, Greece

[2] Ying Li, Guoxiao Guo, and Youyi Wang, "A Nonlinear Control Scheme for Fast Settling in Hard Disk Drives", IEEE Transactions on Magnetics, Vol. 40, No. 4, July 2004, 2086-2088

5. Discrete-time Sliding Mode Control

5.1 Controller Design

In this section, a pure sliding mode control is designed to unify the track-seeking task and track-following tasks into one control scheme, aiming to improve both the transient performance and steady-state performance of HDDs.

The discrete-time nominal model from Benchmark can be written as

$$\begin{aligned} e(k+1) &= Ae(k) + B(u(k) + D(k)) \\ y(k) &= Ce(k) \end{aligned} \tag{5.1}$$

where $A = \begin{pmatrix} 1 & k_y T_s \\ 0 & 1 \end{pmatrix}, B = \begin{pmatrix} k_y k_v T_s^2 / 2 \\ k_v T_s \end{pmatrix}, C = [1 \quad 0], e(k) = \begin{pmatrix} e_1(k) \\ e_2(k) \end{pmatrix}$; $D(k)$ denotes the model uncertainty and disturbance. The sliding surface $s(k) = 0$ is designed as

$$s(k) = H(k)e(k) = \begin{pmatrix} h_1(k) & 1 \end{pmatrix} \begin{pmatrix} e_1(k) \\ e_2(k) \end{pmatrix} = 0 \tag{5.2}$$

If the model is exactly known and there is no disturbance, which means $D(k)$ =0, the controller is designed as

$$u(k) = u_{s1}(k) = -[H(k)B]^{-1}[H(k)A - (1-q)H(k-1)]e(k) \tag{5.3}$$

Plugging Equation (5.3) into Equation (5.1),

$$s(k+1) = (1-q)s(k) \tag{5.4}$$

For $0 < q < 1,\ s(k) \to 0$ as $k \to \infty$, which means the system will approach to the sliding surface and stay on it.

However, in the real case, $D(k)$ is always nonzero. Here it is assumed to be bounded by $|D(k)|< D$.

The controller is designed [2] as

$$u(k) = u_{s1}(k) + u_{s2}(k) \tag{5.5}$$

$$u_{s1}(k) = -[H(k)B]^{-1}[H(k)A - (1-q)H(k-1)]e(k) \tag{5.6}$$

$$u_{s2}(k) = -[H(k)B]^{-1}[D\rho(k) + \varepsilon]\,\mathrm{sgn}(s(k)) \tag{5.7}$$

where $u_{s2}(k)$ is to compensate the uncertainties. Plugging Equations (5.6) and (5.7) into the system, we have

$$s(k+1) = (1-q)s(k) - (\varepsilon + \gamma(k))\,\mathrm{sgn}(s(k)) \tag{5.8}$$

The parameters in Equations (5.5)-(5.7) should satisfy the following conditions

$$\rho(k) > \|H(k)B\| \tag{5.9}$$

$$\varepsilon > 0 \tag{5.10}$$

$$0 < q < 1 \tag{5.11}$$

In Section 5.2, it will be shown that the controller (5.5) - (5.7) can make the system approach to and stay in a specific band centered at the sliding surface.

Additionally, motivated by the idea of approximate time-optimal control, Reference [2] has suggested a method to modify the sliding surface, by setting h_1 an error-based function:

$$h_1(k) = \begin{cases} \sqrt{2k_v \alpha u_{\max} / (k_y |e_1(k)|)} & |e_1(k)| > y_a \\ \sqrt{2k_v \alpha u_{\max} / (k_y y_a)} & |e_1(k)| \le y_a \end{cases} \tag{5.12}$$

The relationship between $h_1(k)$ and $e_1(k)$ is shown in Figure 5.1. Certain advantages can be shown in such a sliding surface. For example, by using $\sqrt{|e_1(k)|}\,\mathrm{sgn}(e_1(k))$ instead of $e_1(k)$, $s(k)$ will not become unexpected large, and thus the control signal would not become unexpected large.

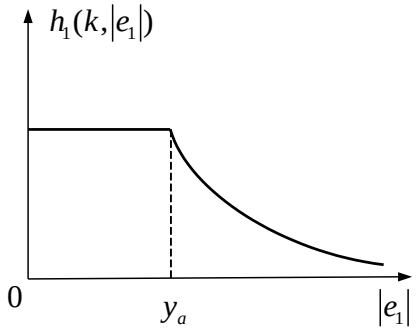

Figure 5.1 $h_1(k)$ and $e_1(k)$

5.2 Stability Analysis

For discrete-time sliding mode control, there are several types of stability conditions from literature.

1). $s(k)\cdot\Delta s(k)<0$ By Dote & Hoft, 1980

2). $|s(k+1)|<|s(k)|$ By Sarpturk, *et al*, 1987

3). $v(k+1)-v(k)<0$ with $v(k)=s^2(k)/2$

Actually (1) is not enough to conclude Lyapunov stability. (2) and (3) are essentially equivalent. Each of them can be explained as this: if $s(k)>0$, $-2s(k)<\Delta s(k)<0$; if $s(k)<0$, $0<\Delta s(k)<-2s(k)$. The two kinds of conditions can ensure that $s(k)$ goes zero. However, it is rather difficult to design a controller to satisfy the conditions (2) or (3). Gao etc., proposed another kind of conditions in 1995 [3], explained as follows.

$$4).\begin{cases}\text{If } s(k)>\Delta, \text{ then } -\Delta \le s(k+1) < s(k)\\ \text{If } s(k)<-\Delta, \text{ then } s(k) < s(k+1) \le \Delta\\ \text{If } |s(k)|<\Delta, \text{ then } |s(k+1)|<\Delta\end{cases}$$

The above equations describe the following conditions

A1. Starting from any initial point, the trajectory will move monotonically toward the switching plane and cross it in finite time

A2. Once the trajectory has crossed the switching plane the first time, it will cross the plane again in every successive sampling period, resulting in a zigzag motion about the switching plane .

A3. The trajectory stays within a specific band.

It is easier to design a controller satisfying condition (4), to ensure that $e(k)$ is bounded. But it does not ensure that $s(k)$ converges to zero.

Through plugging the controller of Equations (5.5)-(5.7) into the system, the following conclusion can be obtained:

$$\begin{aligned}&s(k)>\Delta(k) \Rightarrow -\Delta(k) \le s(k+1) < s(k)\\ &s(k)<-\Delta(k) \;\Rightarrow\; s(k) < s(k+1) \le \Delta(k)\\ &-\Delta(k) \le s(k) < 0 \Rightarrow 0 < s(k+1) \le \Delta(k)\\ &0 < s(k) \le \Delta(k) \;\Rightarrow\; -\Delta(k) \le s(k+1) < 0\end{aligned} \tag{5.13}$$

which means $s(k)$ is bounded by $\Delta(k)$, where

$$\Delta(k) = \frac{\varepsilon + \gamma(k)}{1-q} < \Delta = \frac{\varepsilon+\gamma}{1-q} \tag{5.14}$$

$$\gamma(k) = -H(k)BD(k)\operatorname{sgn}(s(k)) + D\rho(k) < \gamma \tag{5.15}$$

The detailed proof of stability (Equation 5.13) is as follows:

1st: We want to show $s(k)>\Delta(k) \;\Rightarrow\; -\Delta(k) \le s(k+1) < s(k)$

when $s(k) > \Delta(k) = \dfrac{\varepsilon + \gamma(k)}{1-q} > 0$, $\text{sgn}(s(k)) = 1$, Equation (5.8) becomes

$$s(k+1) = (1-q)s(k) - \varepsilon - \gamma(k) > (1-q)\frac{\varepsilon + \gamma(k)}{1-q} - \varepsilon - \gamma(k) = 0$$

$$s(k+1) = s(k) - qs(k) - \varepsilon - \gamma(k) < s(k)$$

Therefore $0 < s(k+1) < s(k)$.

2nd: Similarly, $s(k) < -\Delta(k) \implies s(k) < s(k+1) \le \Delta(k)$

3rd: We want to show $|s(k)| \le \Delta(k) \implies |s(k+1)| \le \Delta(k)$

(a) when $0 < s(k) \le \Delta(k)$,

$$0 < s(k) \le \frac{\varepsilon + \gamma(k)}{1-q}, \text{sgn}(s(k)) = 1, s(k+1) = (1-q)s(k) - \varepsilon - \gamma(k)$$

Therefore

$$s(k+1) \le (1-q)\frac{\varepsilon + \gamma(k)}{1-q} - \varepsilon - \gamma(k) = 0$$

Further,

$$s(k) > 0$$
$$\Rightarrow (1-q)^2 s(k) > 0 \Rightarrow (1-q)^2 s(k) - (\varepsilon + \gamma(k)) > -(\varepsilon + \gamma(k))$$
$$\Rightarrow (1-q)^2 s(k) - (\varepsilon + \gamma(k)) + q(\varepsilon + \gamma(k)) > -(\varepsilon + \gamma(k))$$

$$\Rightarrow (1-q)s(k) - (\varepsilon + \gamma(k)) > -\frac{(\varepsilon + \gamma(k))}{1-q}$$
$$\Rightarrow s(k+1) > -\frac{(\varepsilon + \gamma(k))}{1-q} = -\Delta(k)$$

Therefore, $0 < s(k) \le \Delta(k) \Rightarrow -\Delta(k) < s(k+1) \le 0$

(b) When $-\Delta(k) \le s(k) < 0$,

$$-\frac{\varepsilon + \gamma(k)}{1-q} \le s(k) < 0, \text{sgn}(s(k)) = -1$$

Therefore,

$$s(k+1) = (1-q)s(k) + \varepsilon + \gamma(k) \ge (1-q)(-\frac{\varepsilon + \gamma(k)}{1-q}) + \varepsilon + \gamma(k) = 0$$

Further,

$$s(k) < 0 \Rightarrow s(k+1) = s(k) - qs(k) + \varepsilon + \gamma(k) < \varepsilon + \gamma(k) < \frac{\varepsilon + \gamma(k)}{1-q} = \Delta(k)$$

Therefore $-\Delta(k) \le s(k) < 0 \ \Rightarrow \ 0 \le s(k+1) \le \Delta(k)$

Up to now, the stability proof has been done. The system of Equation (5.1) is stable with the controller of Equations (5.5) - (5.7), under certain constraints of Equations (5.9) – (5.11).

5.3 State Observer

To generate our control signal, we need not only the position signal but also the velocity signal. In real hard disk drives, the only signal we can obtain is PES. Therefore we need to design a state observer to obtain the velocity information.

A full state observer usually has the following form

$$\hat{x}(k+1 \mid k) = A\hat{x}(k \mid k-1) + Bu(k) + L[y(k) - C\hat{x}(k \mid k-1)] \quad (5.16)$$

where $\hat{x}(i \mid j)$ is the estimation for $x(i)$ based on the measurements up to time j .The eigenvalues of $A-LC$ should be all inside of the unit circle for asymptotic stability. Note that the observer does not make use of $y(k)$ to estimate the state $x(k)$.

Another common state observer with predictor and corrector is introduced [4]:

Predictor $\hat{x}(k+1 \mid k) = A_{Ts}\hat{x}(k \mid k) + B_{Ts}u(k)$

Corrector $\hat{x}(k+1 \mid k+1) = \hat{x}(k+1 \mid k) + L_{Ts}[y(k+1) - C_{Ts}\hat{x}(k+1 \mid k)]$

By combining the predictor and corrector, we have

$$\begin{aligned}\hat{x}(k+1 \mid k+1) = (I-LC)A\hat{x}(k \mid k) \\ + (I-LC)Bu(k) + Ly(k+1)\end{aligned} \tag{5.17}$$

5.4 Simulation Results

The whole system for simulation is illustrated in Figure 5.1. The design of the controller is based on the nominal model of HDDs, but the simulation is done based on the full-order model including the notch filters and the whole benchmark disturbance profile.

In the simulation, the reference signal is shown in Figure 5.2. We would like to check whether such a system has a good transient performance (smaller overshoot, short response time, etc), and a good steady-state performance under such kind of reference. The full simulation parameters are listed in Table 5.1.

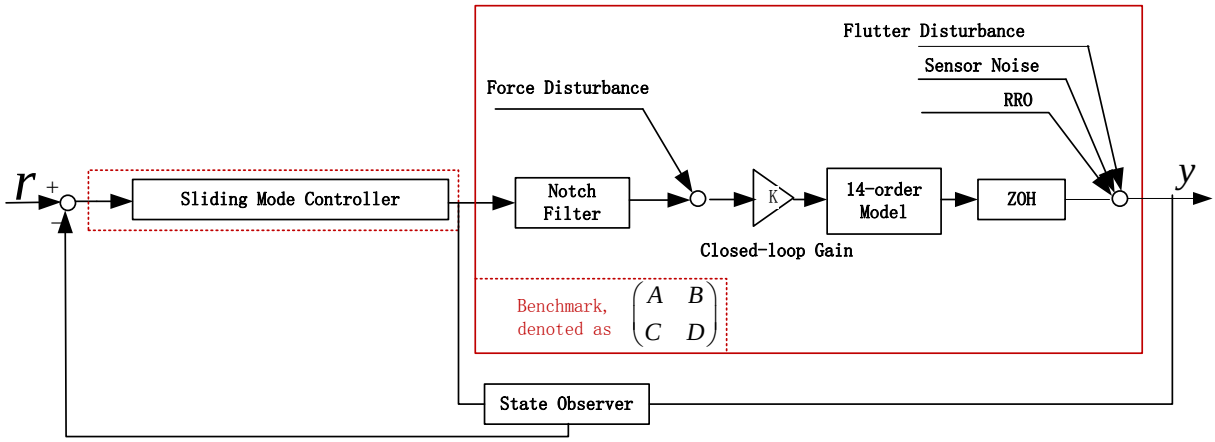

Figure 5.1 Control Scheme

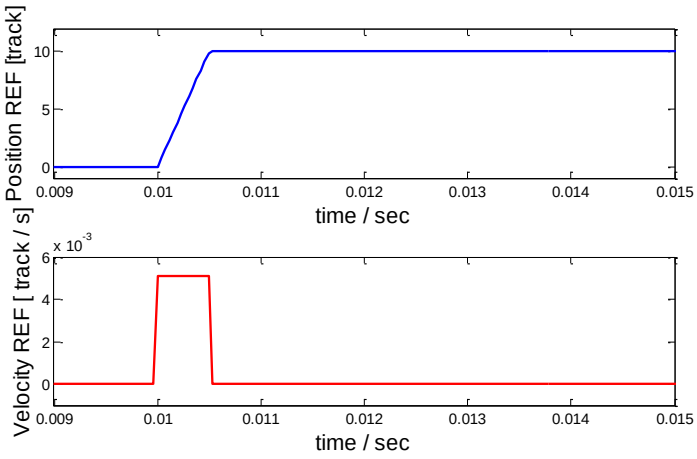

Figure 5.2 Position Reference and Velocity Reference

Table 5.1 Simulation Parameters	
Force Disturbance Bound	$D = 0.001$
Sliding Surface	$\alpha = 0.9996;\ y_a = 1/\text{track};\ \phi = 0.0003$
Controller	$\varepsilon = 1e-5 > 0$ $0 < q = 0.001 < 1$ $\rho(k) = 0.04 > \max(\|H(k)B\|) = 0.039$

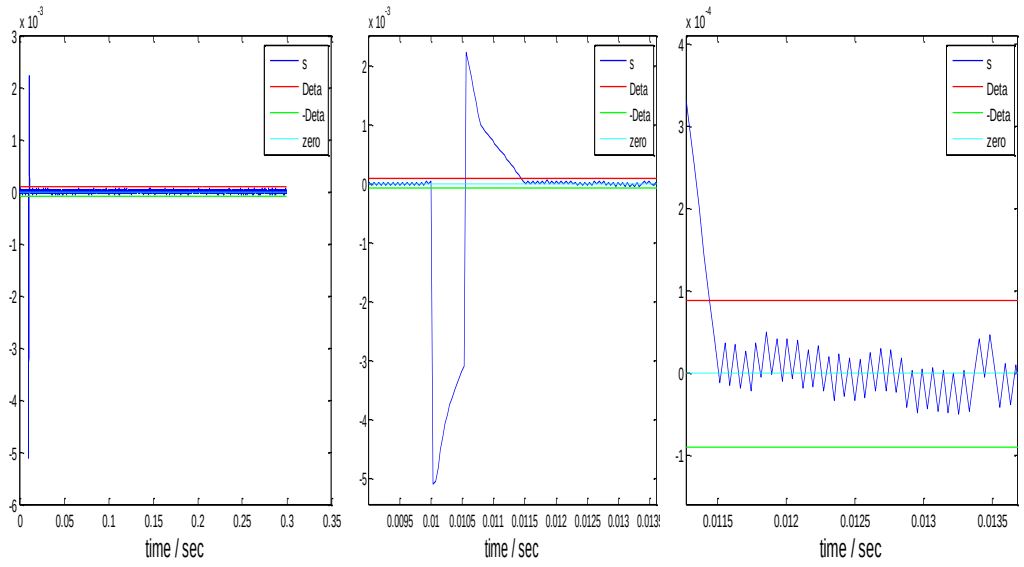

(a) 0s – 0.3s (b) 0.0090s – 0.0135s (c) 0.0110s – 0.0135s

Figure 5.3 Sliding Surface Performance

The simulation results in Figure 5.3 are based on the nominal model with only force disturbance. Figure 5.3 indicates that $s(k)$ approaches to the sliding surface $s(k)=0$ in finite time, and then stay in a specific band. Specifically, Figure 5.3 (c) indicates that $s(k)$ will change its sign every successive sampling period after the system approaches $s(k)=0$.

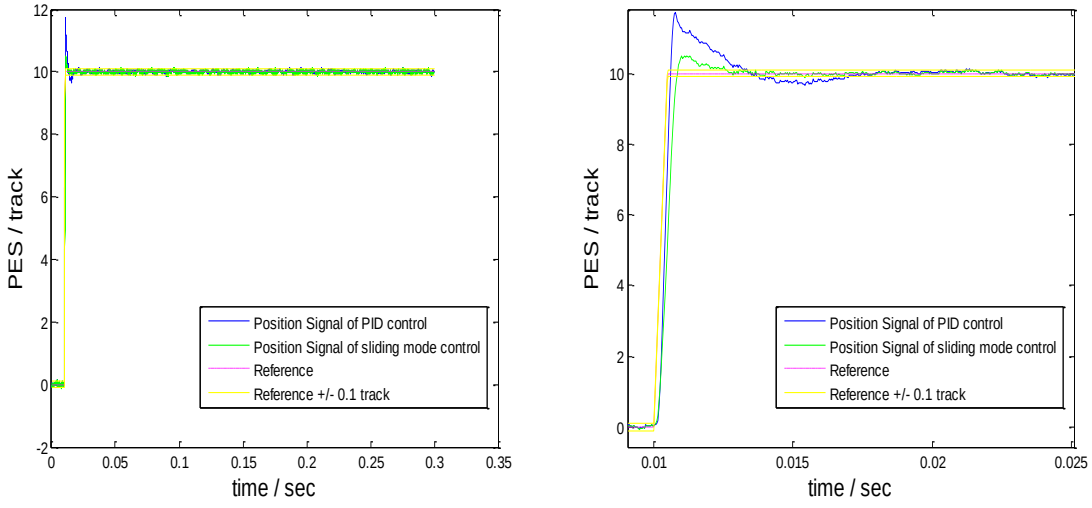

(a) 0s – 0.3 s (b) 0.0095s – 0.025s

Figure 5.4 Position Signal (Transient Performance)

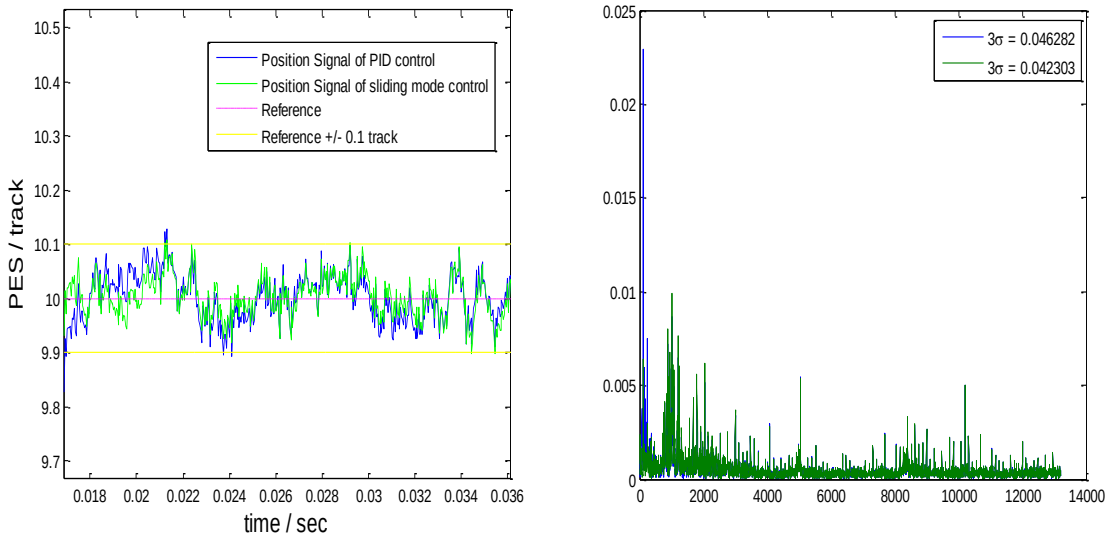

(a). Time Domain (b). Frequency Domain

Figure 5.5 Position Signal (Steady State Performance)

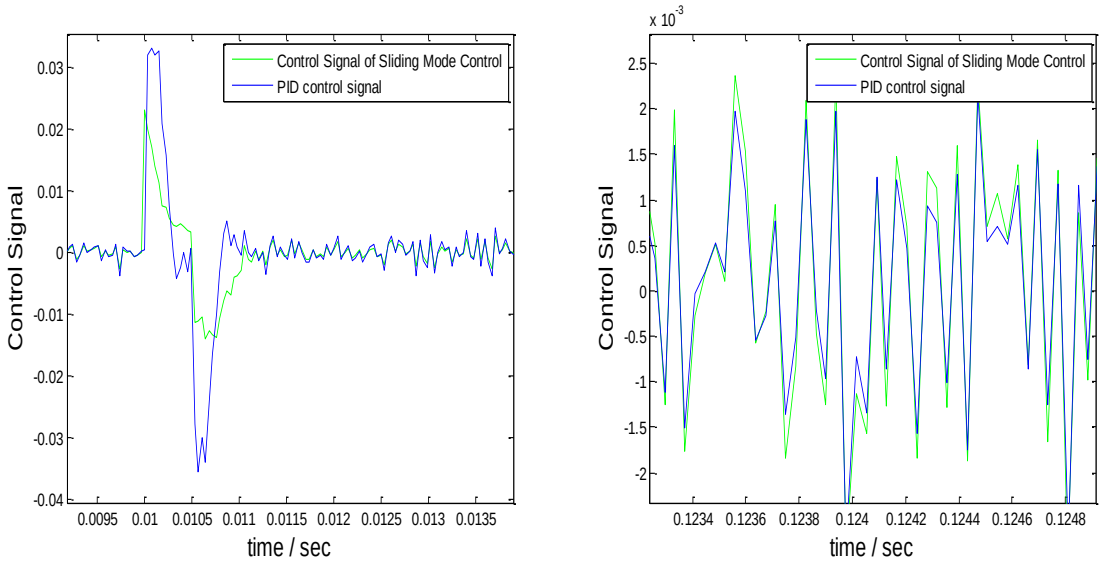

a. Transient Performance b. Steady-state Performance

Figure 5.6 Control Signal

The simulation is based on the full-order model from Benchmark with full disturbance profile. Figures 5.4-5.6 compare the results of the sliding mode control and the PID controller provided in Benchmark. The results indicate that the sliding mode control has improved both the transient performance (overshoot and response time), and the steady-state performance (3Sigma value of PES).

References

[1] Qinglei Hu, Chunling Du, Lihua Xie, and Youyi Wang, "Discrete-time Sliding Mode Control With Time-varying Surface for Hard Disk Dirves," IEEE Transactions on Control Systems Technology, Vol. 17, No. 1, January 2009, 175-183.

[2] D.Zhang and G.Guo, "Discrete-time sliding mode proximate time optimal seek control of hard disk drives," IEE Proc.-Control Theory Appl., Vol. 147, No. 4, July 2000, 440- 446.

[3] Weibing Gao, Yufu Wang, and Abdolah Homaifa, "Discrete-Time Variable Structure Control Systems," IEEE Transactions on Industrial Electronics, Vol.42, No.2, April 1995, 117-122.

[4] ME232 class notes of UC Berkeley, Advanced Control System I, Professor Tomizuka

6. Preliminary Study on multi-rate nonlinear control for HDDs

In section 5, a discrete-time sliding mode control is designed; both the transient performance (smaller overshoot and reduced response time) and the steady-state performance (smaller 3Sigma value of PES) have been improved. In this section, we focus on the track-following process and try to improve the steady-state performance by implementing such a sliding mode controller into a multi-rate system.

6.1 HDD system with increased servo sector numbers

The motivation to study a HDD system with more servo sectors is to evaluate the discrete time sliding mode control scheme for different sampling periods. In the Benchmark Model, the servo sector number is 220. In this section, we revise the model by increasing the servo sector number to 440. An increased servo sector number results in a higher PES sampling rate. The parameters for the original Benchmark model and the revised model are listed in Table 6.1.

Table 6.1 System Parameters

Number of servo sectors per track	**440 servo sectors per track**	**220 servo sectors per track**
Rotational Speed	$r = 7200$	
k_y	$k_y = 3.937\times10^{6}\ \text{track}\cdot\text{m}^{-1}$	
k_v	$k_v = 951.2\ \text{ms}^{-2}\text{A}^{-1}$	
Width of Track	$T_p = 2.54e\times10^{-7}\ \text{m}$	
PES Sampling Rate	$T_{s1} = 1.8939\times10^{-5}\ \text{s}$	$T_{s2} = 3.7879\times10^{-5}\ \text{s}$
Force Disturbance Sampling Rate	$T_{s2}/2$	$T_{s2}/2$
RRO Sampling Rate	T_{s2}	T_{s2}
Sensor Noise Sampling Rate	T_{s2}	T_{s2}
Flutter Disturbance Sampling Rate	T_{s2}	T_{s2}

First we try to find the equivalent system for different sampling rate. Considering the real dynamics of the system (Equation 5.17), we have

$$\frac{s(k+1)-s(k)}{T_s} = -\frac{q}{T_s}s(k) - \frac{\varepsilon}{T_s}\mathrm{sgn}(s(k)) - \frac{\gamma(k)}{T_s}\mathrm{sgn}(s(k)) \tag{6.1}$$

where $\gamma(k) = -H(k)BD(k)\mathrm{sgn}(s(k)) + D\rho(k)$. Note $\gamma(k)$ contains uncertainty $D(k)$.

To ensure

$$\frac{s(k+1)-s(k)}{T_{s1}} = \frac{s(k+1)-s(k)}{T_{s2}} \tag{6.2}$$

the following equation should be maintained:

$$\frac{q_1}{T_{s1}} = \frac{q_2}{T_{s2}}; \frac{\varepsilon_1}{T_{s1}} = \frac{\varepsilon_2}{T_{s2}}; \frac{\gamma_1(k)}{T_{s1}} \approx \frac{\gamma_2(k)}{T_{s2}} \tag{6.3}$$

The parameters for the two approximately equivalent systems are listed in Table 6.2.

Table 6.2 Control Parameters

Number of servo sectors per track	**440 servo sectors per track**	**220 servo sectors per track**
Force Disturbance Bound	$D = 0.001$	
Sliding Surface	$\alpha = 0.9996$; $y_a = 1$ / track; ϕ=0.0003	
Plant Parameters	$A_{Ts_1} = \begin{pmatrix} 1 & k_y T_{s1} \\ 0 & 1 \end{pmatrix}$ $B_{Ts_1} = \begin{pmatrix} k_y k_v T_{s1}^{\ 2}/2 \\ k_v T_{s1} \end{pmatrix}$	$A_{Ts_2} = \begin{pmatrix} 1 & k_y T_{s2} \\ 0 & 1 \end{pmatrix}$ $B_{Ts_2} = \begin{pmatrix} k_y k_v T_{s2}^{\ 2}/2 \\ k_v T_{s2} \end{pmatrix}$
Observer	$\lambda\{(I - L_{Ts_1}C_{Ts_1})A_{Ts_1}\} = \left(\lambda\{(I - L_{Ts_2}C_{Ts_2})A_{Ts_2}\}\right)^{\frac{1}{2}}$	
Controller Parameters	$\varepsilon_1 = \varepsilon_2/2 > 0$	$\varepsilon_2 = 1e-5 > 0$
	$0 < q_1 = q_2/2 = 0.0005 < 1$	$0 < q_2 = 0.001 < 1$

	$\rho_1(k) = 0.019 + 0.001$ $> \max \left\| H_1(k) B_{T_{S_1}} \right\| = 0.019$	$\rho_2(k) = 0.039 + 0.001$ $> \max \left\| H_2(k) B_{T_{S_2}} \right\| = 0.039$

Simulations have been done for the two systems with 220 servo sectors and 440 servo sectors respectively. As shown in Figure 6.1, the system with 440 servo sectors has a reduced 3Sigma value of PES. This implies that, if the sampling rate of the PES can be increased, the control signal could be updated faster, and the 3Sigma of PES can be reduced effectively.

However, in the real HDD system, the PES sampling rate is highly restricted. Therefore, we would like to implement the discrete-time sliding mode control into a Multi-rate System. The basic idea, as shown in Figure 6.2, is to update the control signal faster than PES sampling rate.

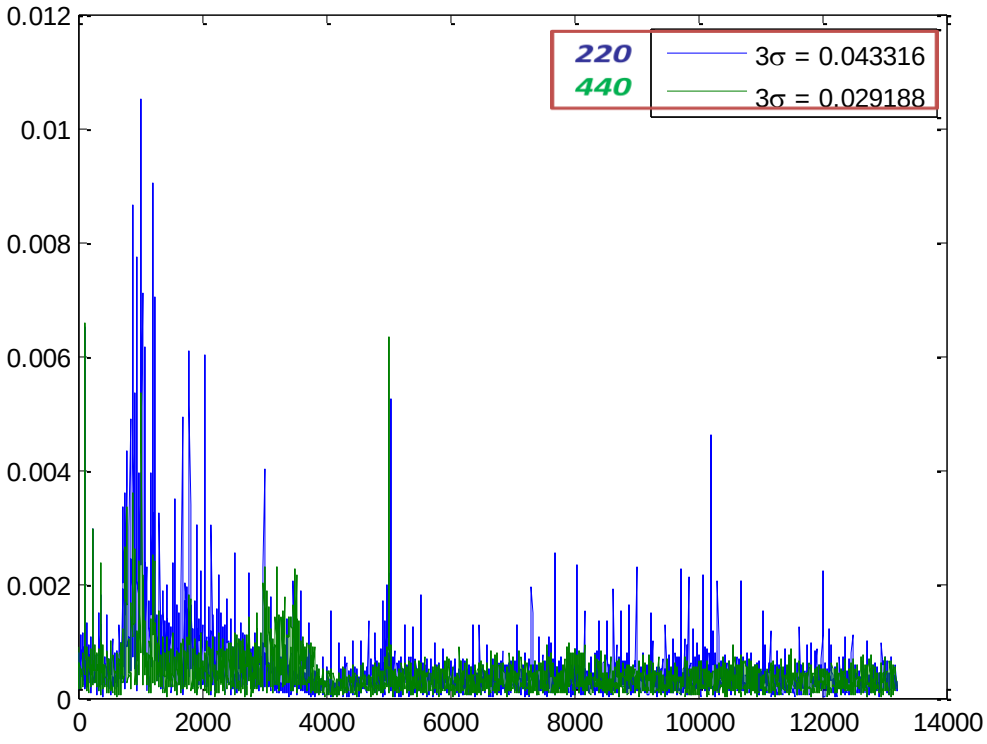

Figure 6.1 3Sigma Value of PES

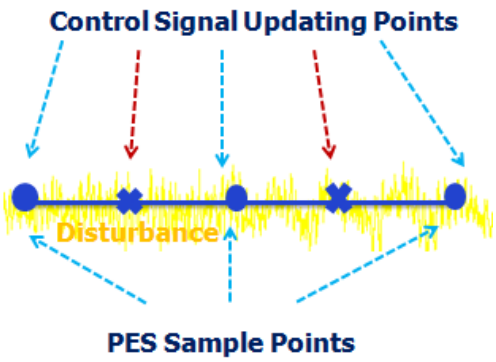

Figure 6.2 Basic Idea for Multi-rate Control

6.2 Multi-rate System and Multi-rate State Observer

To update our control signal faster than PES sampling rate, a multi-rate system needs to be build. As shown in Figure 6.3, it includes a fast sampling segment (the controller and the state observer) and a slow-sampling segment (the plant).

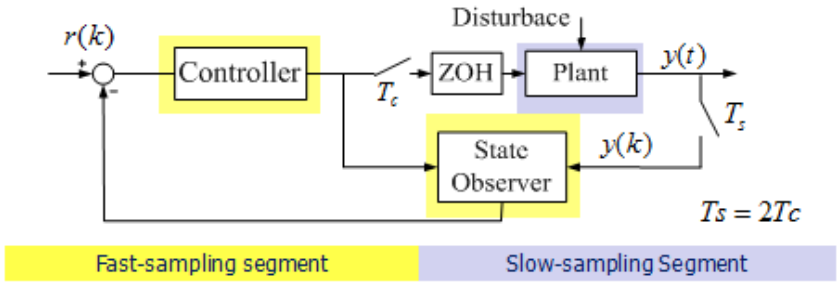

Figure 6.3 Multi-rate Control System

This means, some information of PES at inter-sampled points is required to update the control signal. For example, if the control signal updating period T_c is half of the PES sampling period T_s, i.e., $T_c = 0.5T_s$, the PES information is required to update the control signal every T_c. But PES is measured every T_s. Therefore, a multi-rate state observer is necessary to obtain the PES estimation at the inter-sampled points.

Such an observer uses one-step prediction based on the nominal model to update our control signal. The whole equations are listed as follows.

$$\begin{aligned}\hat{x}(k+0.5\,|\,k) &= A_{Tc}\hat{x}(k\,|\,k) + B_{Tc}u(k)\\ \hat{x}(k+1\,|\,k+1) &= (I - L_{Ts}C_{Ts})A_{Ts}\hat{x}(k\,|\,k) + (I - L_{Ts}C_{Ts})B_{Ts}u(k) + L_{Ts}y(k+1)\end{aligned} \tag{6.4}$$

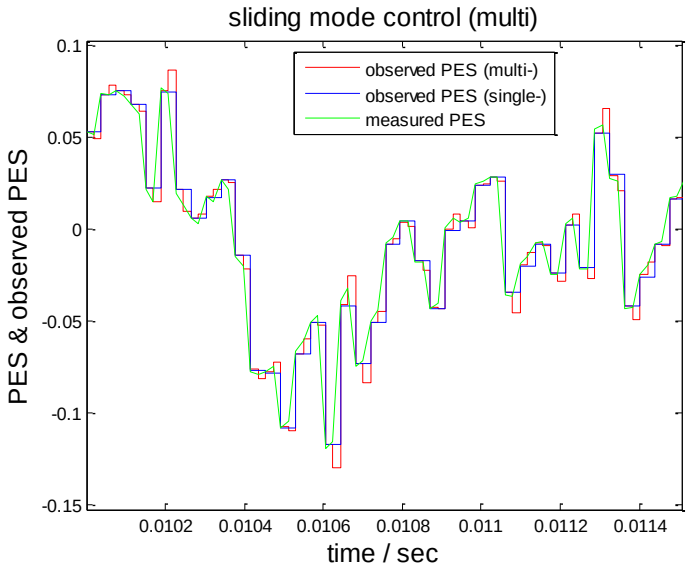

Figure 6.4 State Observer (Single-rate observer and Multi-rate observer)

Figure 6.4 provides the simulation and indicates how such an observer works. It includes the measured PES, the observed PES by single-rate state observer, and the observed PES by multi-rate observer. As shown in the simulation result, better estimation of PES can be acquired through the multi-rate observer at most inter-sampled points, while even worse estimation of PES is acquired at other inter-sampled points.

7. Conclusion

In this project, two kinds of nonlinear algorithms have been proposed and analyzed.

The first algorithm is nonlinear PID combined with the sliding mode control. The sliding mode control works when PES is large and is turned off when PES is small. Furthermore, the nonlinear PID is reduced to a linear PID as PES becomes small. Simulation results show that such an algorithm can obtain fast transient performance and good steady-state performance. However, this algorithm involves lots of efforts on parameter tuning. Stability analysis is also difficult for this algorithm.

The second algorithm is a pure discrete-time sliding mode control. It combines the track-seeking task and track-following task into one control scheme. A boundary layer is introduced to mitigate the chatter and stability analysis is provided to ensure a bounded tracking error. Simulation results show that such a pure sliding mode control can also obtain a fast transient performance during the track-seeking process and keep the 3Signma value of PES small during the track-following process.

Additionally, some preliminary study on multi-rate system has been done and a multi-rate observer has been designed. In the future, we would like to implement such a discrete-time sliding mode control into a multi-rate control system, to further enhance the track-following performance of HDDs.